MetaResonance—A Reconfigurable Surface for Holographic Wireless Power Transfer

Kai Li, M. Yousof Naderi, Ufuk Muncuk, and Kaushik Roy Chowdhury, *Senior Member, IEEE*

***Abstract*—This article presents a design and systems level implementation of a magnetic resonance-based wireless power transfer system with a novel *metasurface* layer. This layer shapes the magnetic field through it that results in "MetaResonance." This phenomenon is key in transforming an existing surface into an intelligent wireless charger for the following: 1) reconfigurable and on-demand energy shaping that can customizable energy hologram; and 2) beamforming to charge multiple devices. The advantages of MetaResonance over conventional methods such as inductive and magnetic resonance charging, distributed RF and magnetic beamforming, and energy hopping lie in its ability to provide high-power delivery with safety guarantees, high end-to-end efficiency, and customized power distribution profile in three dimensions over the surface. From a systems implementation viewpoint, we achieve this through a power distribution layer at the bottom and the MetaResonance cell array layer at top. We have simulated, fabricated, and built an experimental setup of the proposed MetaResonance wireless power transfer system. Performance results demonstrate the reconfigurability in the power and energy fields over the whole surface with fine granularity. Specifically, the magnetic field can be blocked within 2 cm with more than 95% efficiency while the power transfer efficiency can be improved up to 92.8% by beamforming. We have demonstrated various real-world charging applications concerning consumer electronics, industrial tools, battery packs, and medical device wireless charging.**

***Index Terms*—Magnetic resonance, MetaSurface, strong coupling, wireless power transfer.**

I. Introduction

WIRELESS power transfer for consumer devices, drones, robots, and other mobile systems relies on creating an adaptive electromagnetic field that can charge at-a-distance and thereby eliminate the inconvenience of wired charging solutions. Strongly coupled magnetic resonance enables wireless power transfer over a distance of several meters via intermediate resonating coils placed between a transmitter and receiver coil pair [1]. Various related wireless power transfer systems, such as domino resonator [2], [3], energy hopping [4]–[6], MagMIMO [7], [8], and metasurface-based [9]–[11] systems have been proposed that further extend the transfer distance (to 2 m), increase charging area (to 0.5×0.75 m^2), and improve the spacial resolution (in cm) of charging. Metasurface, i.e., a surface composed of artificially constructed materials, stands out among these different options [12], [13]. Given the ability to control the incident electromagnetic field propagation, such metasurfaces are now widely used in different areas like nanophotonics [14], [15], plasmonics [16]–[18], wireless communication [19] in the GHz band [20] and medical applications [20]. In context of the wireless power transfer application, prior work involving metasurfaces focuses on increasing the range of wireless power transfer and the charging power available at one specific spot [21]. These methods are not amenable to activating multiple charging spots and do not address the potential safety issues related to the proximity of magnetic fields to human tissue. In addition, the current inductive and magnetic resonance coil based charging architectures [22] create a power distribution that has a fixed concentric pattern with the maximum intensity of energy field maximum at the center that gradually decreases moving radially outwards. In summary, the key challenges associated with conventional wireless power transfer approaches are lack of flexible power distribution over the surface, blind spots, and magnetic field leakages that can result in interference and human safety issues. This article introduces MetaResonance wireless power transfer, the first-of-its-kind system that enables creation of fully reconfigurable energy patterns over a surface. It is able to shape the energy fields with high granularity allowing power amplification, pass-through, and blocking, as needed. The MetaResonance wireless power transfer architecture is shown in Fig. 1. There are two layers, with the bottom layer being the power distribution layer and top layer is MetaResonance control layer. Here, the power layer is an array of identical transmitter coil resonators where the power propagates to different resonator via energy hopping [4]. Here, only one power amplifier, called the source transmitter, would be connected to one transmitter coil. The rest of the transmitter coils get power from the source transmitter through the magnetic resonant mutual coupling between adjacent transmitters. Our previous works [4], [5] discuss and explain the energy hopping architecture, design, and performance results for surface-based charging.The meta-resonance layer that is introduced in this work is a critical element in providing safety, high end-to-end efficiency, and power amplification for a high-performance and practical surface-based wireless charging

Manuscript received 18 March 2022; revised 30 May 2022; accepted 17 June 2022. Date of publication 7 July 2022; date of current version 3 January 2023. This work was supported by the funds available through the US National Science Foundation under Grant CNS 1452628. *(Corresponding author: Kai Li.)*

The authors are with the Electrical and Computer Engineering Department, Northeastern University, Boston, MA 02115 USA (e-mail: ka.li@northeastern.edu; m.naderi@northeastern.edu; u.muncuk@northeastern.edu; krc@ece.neu.edu).

Color versions of one or more figures in this article are available at https://doi.org/10.1109/TIE.2022.3187570.

Digital Object Identifier 10.1109/TIE.2022.3187570

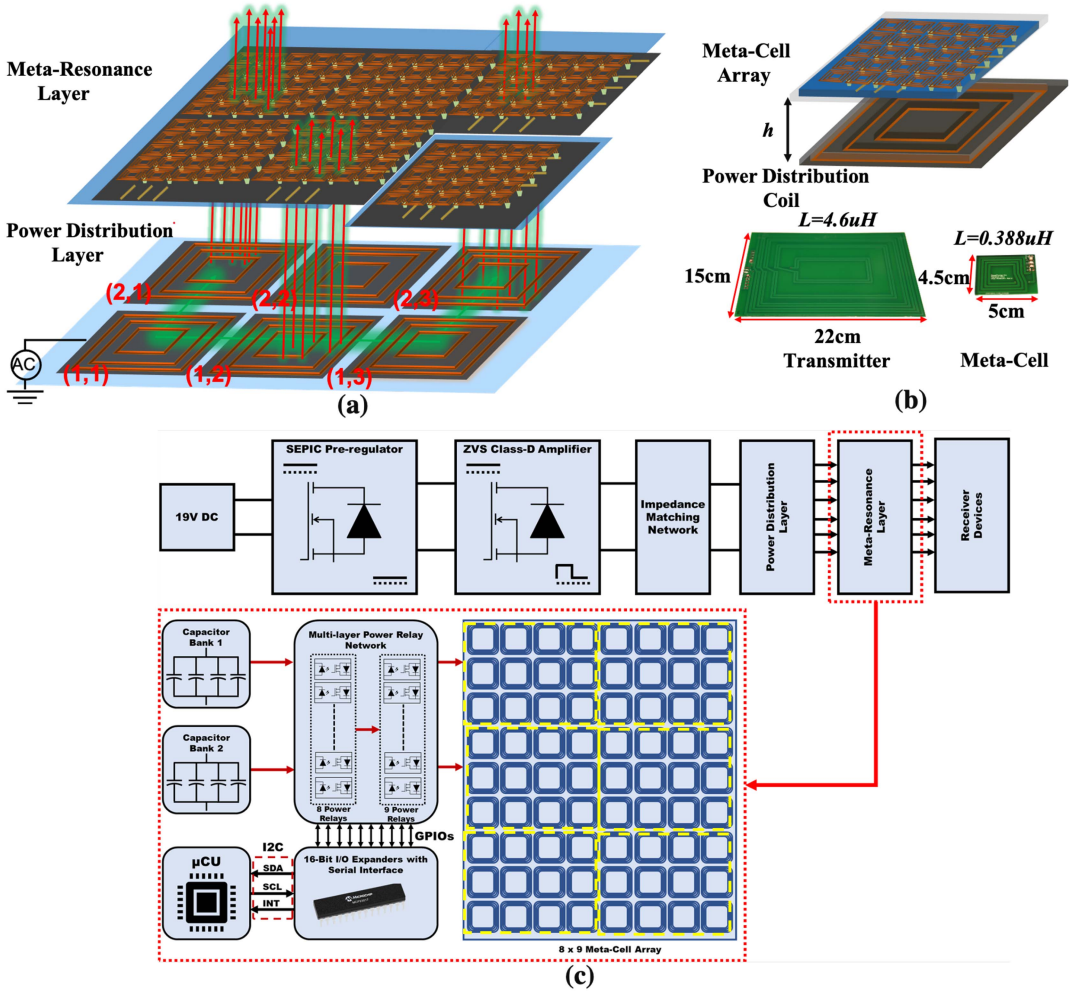

Fig. 1. Architecture of MetaResonance wireless power transfer system. (a) Two-layer architecture; the bottom layer does power distribution with multiple transmitter coils and the top layer is a MetaResonance layerwith an array of meta-cells, (b) one MetaResonance unit with one transmitter coil at bottom and meta-cell array at top, and the fabricated transmitter and meta-cell, and (c) block diagram of the MetaResonance wireless power transfer system.

system. On the other hand, the control layer consists of a configurable array of meta-cell coils, where each meta-cell is a power cavity resonator that reshapes the energy field passing through it. This article presents the theory behind MetaResonance and then validates it with extensive simulation and experimental results, along with real-world charging applications.

II. MetaResonance Wireless Power Transfer Architecture

Fig. 1(a) shows the overview of the overall MetaResonance wireless power transfer system. The power flows through *energy hopping* between transmitters at the bottom layer over different paths. The specific routing path for the power relay is activated by choosing the impedances of bottom layer transmitter coils [4] (shows via green lines). Furthermore, the power passes through the array of meta-cell coils in the upper layer, where it can be amplified, passed through without any change, and blocked (shown with longer, shorter, and no red lines, respectively).

Fig. 1(b) shows one MetaResonance unit for the wireless power transfer setup, where "h" is the gap separation between bottom and top layers. Here, the transmitter coil is fabricated on FR4 material, with size 15 cm $\times$ 22 cm, the measured inductance is 4.6 μH, and the quality factor is 335. Meta-cell is fabricated on FR4 material, with 4.5 cm $\times$ 5 cm, the measured inductance is 0.388 μH, and the quality factor is 165. Fig. 1(c) shows the block diagram of the MetaResonance wireless power transfer system designed with the goal of at-scale and low-cost implementation. In the power distribution layer, we use a zero voltage switching (ZVS) class-D power amplifier that operates at 6.78 MHz. The power amplifier is powered by a 19 V dc power supply with a single-ended primary-inductor converter (SEPIC) preregulator. Impedance matching network provides the maximum power delivery from the ZVS power amplifier to the transmitter coil. In the meta-resonance layer, we use a meta-cell layer, in which 72 meta-cells are placed in an 8×9 grid forming a meta-cell array. Each meta-cell is separated with a spacing of 0.5 cm to minimize magnetic interference between neighboring meta-cells. Furthermore, each cell is connected to

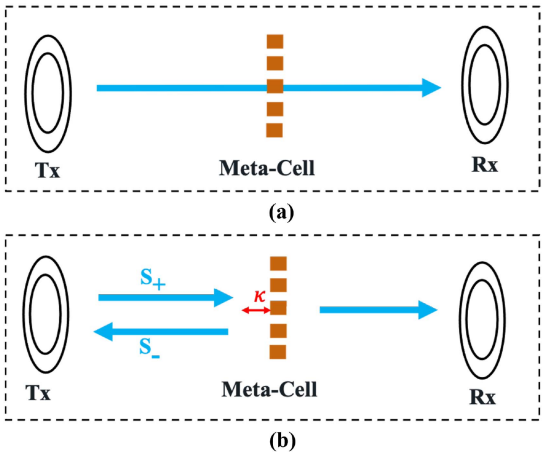

Fig. 2. Theoretical model of MetaResonance wireless power transfer system. (a) Meta-cell as open voltage without coupling and no capacitor. (b) Meta-cell as closed circuit with coupling and connected capacitor.

capacitor banks that can vary the impedance of the meta-cell via a multilayer power relay network. We use Omron G3VM-101CR single-pole single-throw solid-state relay with high isolation between switch input and outputs, and low insertion loss as an element of the multilayer power relay network. The solid-state relays establish a serial electrical connection between each meta-cell coil that is usually open-circuit and the capacitors to firstly create a closed-loop circuit configuration to resonate meta-cell coil and control the case of coupling between the power distribution layer and receiver layer, and then shape the energy field with allowing power amplification, pass-through, and blocking needed. μCU orchestrates all components in the meta-resonance layer and controls 16-b I/O expanders via I2C communication to establish a connection between each meta-cell and capacitor banks through power relay network in order to customize energy patterns over the surface. The customized energy pattern over surface of meta-cell array can be created by tuning the capacitance of meta-cell while the power is passing through to block, amplify, and just pass the power based on the its capacitance value.

III. Theory of Holographic Wireless Power Transfer

This section presents the theory of holographic wireless power transfer. Toward this, we study two cases to discuss the functionality and theory of meta-resonance layer. The first case involves setting a meta-cell coil to open circuit without connecting to a capacitor, as shown in Fig. 2(a). The second case involves each meta-cell being closed circuit with connected capacitors, as shown in Fig. 2(b). In the first case, the meta-cell with open circuit has negligible interference or impact [23] on the power transfer from the transmitter to receiver coils due to the following three factors: 1) a relative low working frequency of 6.78 MHz; 2) large gap-distance (1 cm) of two ends in each meta-cell; 3) low power application of less than 30 W. Thus, the system is similar to the case without any meta-resonance layer, i.e., same as conventional power transfer with one transmitter and one receiver. The theory for this case is well studied [24], [25].

In the second case, the meta-cell is closed circuit with a connected capacitor. Thus, the power from the transmitter is first transferred to each meta-cell with magnetic resonant coupling. Then, the power in each meta-cell is transferred to the receiver coil. During the electromagnetic energy propagation, each meta-cell can control and impact a part of energy from the transmitter coil, which then impacts the power delivery to the receiver. Accordingly, an array of meta-cells between the transmitter coil and receiver coil can shape and control the energy pattern with fine granularity. In this model, as shown in Fig. 2(b), κ determines the coupling rate between the power (wave) from the transmitter coil and the meta-cell. This mutual coupling between transmitter and meta-cell is a function of distance, coil alignment and the relative orientation angle between the two resonators. The power transfer optimization can be explained by wave transmission optimization.

As shown in Fig. 2(b), each square block represents one meta-cell, which can be depicted as a simple LC circuit, L and C are the inductance and capacitance of the meta-cell. Assuming continuous energy circulating in lossless LC circuit, the transient response of voltage($v(t)$) and current($i(t)$) can be represented as

$$v(t) = L\frac{di}{dt}, \quad i(t) = -C\frac{dv}{dt} \tag{1}$$

by combining these two equations, we can get

$$\frac{d^2v}{dt^2} + \omega_0^2 v = 0, \quad \omega_0^2 = \frac{1}{LC} \tag{2}$$

and the time-dependent solution of voltage and current are

$$v(t) = |V|cos(\omega_0 t + \phi), \quad i(t) = \sqrt{\frac{C}{L}}|V|sin(\omega_0 t + \phi) \tag{3}$$

here, $|V|$ is the peak amplitude of the voltage in the LC circuit, and ϕ is the phase change of voltage and current.

However, the above equations are two coupled first-order differential equations, which increases the complexity of calculating the reflection coefficient. Here, we define the complex variables a that consists of two uncoupled first-order differential equations, expressed as

$$a = \sqrt{\frac{C}{2}}\left(v + j\sqrt{\frac{L}{C}}i\right). \tag{4}$$

Substitute $v(t)$ and $i(t)$ of (4) with (3), we can obtain in the steady state

$$a = \sqrt{\frac{C}{2}}[|V|cos(\omega_t + \phi) + j|V|sin(\omega_0 t + \phi)] = \sqrt{\frac{C}{2}}Ve^{j\omega_0 t}. \tag{5}$$

Then, $a(t)$ has the dependence $e^{j\omega_0 t}$, and we note that the energy inside this circuit can be obtained

$$|a|^2 = \frac{C}{2}|V|^2. \tag{6}$$

Hence, the complex variable a is the mode amplitude of the lossless LC circuit, due to the dependence of $e^{j\omega_0 t}$, the resonant

mode of the energy circulating in lossless LC circuit can be fully described by the following:

$$\frac{da}{dt} = j\omega_0 a. \tag{7}$$

If the circuit is lossy, (7) is modified as

$$\frac{da}{dt} = j\omega_0 a - \left(\frac{1}{\tau_o} + \frac{1}{\tau_e}\right) a \tag{8}$$

where $\frac{1}{\tau_o}$ and $\frac{1}{\tau_e}$ are the decay rate due to the loss the radiation rate. As shown in Fig. 2, meta-cell get extra power from transmitter with incident energy wave (amplitude S_+). Without loss of generality, we consider $S_+(x, y)$ as S_+, where (x,y) is a given location on the surface. Given the incident energy wave (S_+) with coupling rate κ, (8) is modified as

$$\frac{da}{dt} = j\omega_0 a - \left(\frac{1}{\tau_o} + \frac{1}{\tau_e}\right) a + \kappa S_+. \tag{9}$$

Here, the incident energy wave come from the transmitter source with working frequency ω, then $S_+ \propto e^{j\omega t}$ with applying perturbation [1], [26], [27]. Thus, at steady state (working frequency would not change at meta-cell), we can find by solving (9)

$$a = \frac{\kappa S_+}{j(\omega - \omega_0 + [(1/\tau_0) + (1/\tau_e)])}. \tag{10}$$

Next, under the consideration of $\frac{1}{\tau_o} = 0$, the functional relation between coupling rate and the radiation rate are calculated based on the theorem of energy conservation, we can get [26]–[28]

$$\frac{d}{dt}|a|^2 = -\frac{2}{\tau_e}|a|^2 = -|S_-|^2, \kappa = \sqrt{\frac{2}{\tau_e}}. \tag{11}$$

As shown in Fig. 2(b), the incident energy wave S_+ will have reflected energy wave S_- after passing through a meta-cell, and it is easy to get that

$$S_- = -S_+ + \kappa a. \tag{12}$$

The power ratio between the delivered power to the devices and the power passing/entering into the meta-cell from source resonator is proportional to the reflection coefficient, defined as the ratio between S_- and S_+. Then, the power reflection coefficient of each meta-cell in the steady is expressed [28], [29] as

$$\eta = \left|\frac{S_-}{S_+}\right|^2 = \left|\frac{\kappa^2}{j(\omega - \omega_0) + \frac{1}{\tau_o} + \frac{1}{\tau_e}} - 1\right|^2. \tag{13}$$

For the magnetic resonance based wireless power transfer, $\frac{1}{\tau_o} = \frac{1}{\tau_e} = \omega/2Q$ are considered [1], [26], [27], Q is the quality factor of meta-cell. Accordingly, the power reflection is only the function of the self-resonant frequency $\omega_0 = 1/\sqrt{LC}$. The capacitance value C is the only variable that is reconfigurable during the operation of the wireless power transfer. Fig. 3 demonstrates the reflection coefficient change with different value of connected capacitor, where it has range [0,1]. Based on reflection coefficient range, the energy transmission performance can be classified strong coupling (($\eta = 0$)) and partial coupling ($0 < \eta < 1$). In the case of strong coupling ($\eta = 0$), each meta-cell acts as a resonator relay, maximizing the power transfer efficiency between transmitter and devices. In the case of partial coupling ($0 < \eta < 1$), the transmitted power is reflected back with different scales. In practical application, the reflection coefficient with $\eta > 0.98$ is considered safe to the human tissue, which is the power blocking via reflecting all of the energy and no power passes through the resonator. By analyzing (13), we find that the reflection coefficient is a function of the parameters $\kappa, \tau_0, \tau_e, \omega, \omega_0$. These parameters are independent with the location over the meta-cell surface, which proves that the energy transmission efficiency is location independent. However, the input power from the transmitter to the meta-cell is location-dependent $P_T(x, y)$[30], which results in the power delivered to the receiver is location-dependent $P_{mc}(x, y)$, expressed as

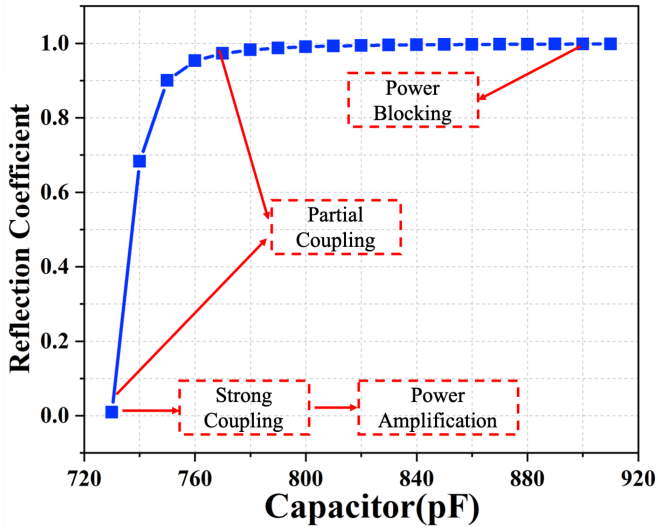

Fig. 3. Reflection coefficient change with different connected capacitors.

$$P_{mc}(x, y) = (1 - \eta)P_T(x, y),\ P_T(x, y) = |S_+(x, y)|^2. \tag{14}$$

With (14), the received power distribution at any position over the meta-cell layer can be obtained given the input power $P_T(x, y)$. In this work, we utilize strong coupling with $\eta = 0$ and partial coupling with $\eta > 0.98$ to amplify and block the power delivery, respectively. Thus, given the reflection coefficiency of meta-cell, we can realize different delivery modes such the power amplifying, power blocking, and normal pass-through of power, all by tuning the connected capacitors for each meta-cell.

IV. Performance Analysis of MetaResonance Wireless Power System

In this section, we provide extensive simulation and experimental results on a real-time MetaResonance wireless power transfer system. In particular, we show the fabricated circuit hardware, transmitter coil, reference coil, meta-cell, receiver coil, the customized receiver with different voltage output, and the class D amplifier. Second, we study the performance of an individual MetaResonance unit and then build a large MetaResonance surface consisting of multiple such units. For each case,

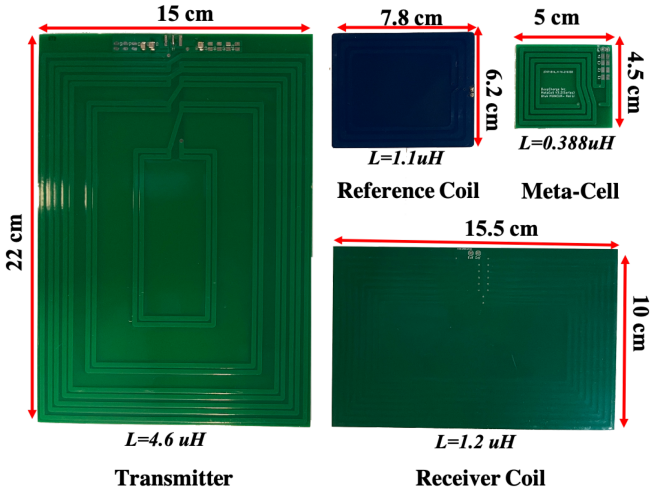

Fig. 4. Fabricated coils for transmitter at the power distribution layer, reference coil for voltage and power measurement, meta-cell at meta-resonance layer, and receiver coil for power measurement at multiple meta-resonance units.

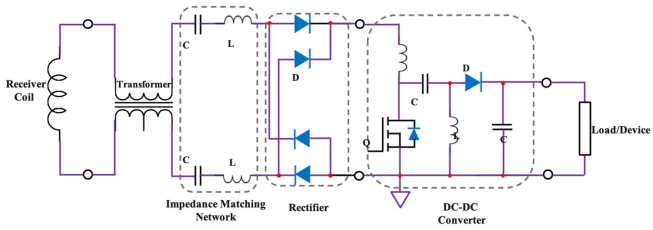

Fig. 5. Power receiver circuit schematic.

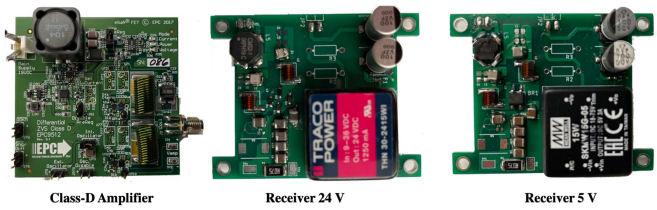

Fig. 6. Class-D amplifier and receiver with different output voltages.

we present the performance results in form of COMSOL simulation. We also provide experimentally observed magnetic field distribution obtained via oscilloscope and the received power on the load (resistor) measured by multimeter. Finally, we demonstrate multiple real-world charging applications including tablet, phone, blood pressure monitor, portable batteries, and power bank surface charging using such a MetaResonance surface.

A. System Design and Fabrication

We designed and fabricated our coils including transmitter coil in the power distribution layer, the meta-cell in meta-resonance layer, the reference coil, and receiver coil using commercial PCB design software EAGLE. Fig. 4, shows the fabricated coil used in the experiments.

The transmitter coil used at the power distribution layer has dimension 22 × 15 cm with inductance $L = 4.6\mu$H. The reference coil is of size 7.8 cm × 6.2 cm with inductance $L = 1.1\mu$H and is fabricated for two usages. The first usage is to measure the voltage through meta-resonance layer with a coil as open circuit, where the corresponding experiment is conducted for both individual MetaResonance unit and multiple MetaResonance units. The reference coil and oscilloscope are serially connected as a close circuit during the measurement. The input resistance of the oscilloscope is $1M\Omega$, which provides high accuracy in measuring the open-circuit voltage of the reference coil. We repeat the measurement 20 times for each trial to accurately measure the open-circuit voltage of the reference coil. The second usage is to measure the received power to the load in the experiment of an individual MetaResonance unit. The reference coil is connected to the receivers, unlike the first usage measurement, as shown in Fig. 6. We design an impedance matching network to accurately ensure the maximum power transfer between the reference coil and the rectifier circuitry at receivers. We connect a power resistor that can keep its resistance identical with up to 100 W of its power to the receiver's output as load. We use a precision multimeter with more than 99% of accuracy to measure the voltage of the load. We also repeat the measurement 20 times for each test trial as the first experimental setup. In addition, the meta-cell coil for the cell array of the meta-resonance layer is of size 5 cm × 4.5 cm and inductance $L = 0.388\ \mu$H. Last, the receiver coil in Fig. 4 is used to measure the received power of the load in the experiment involving multiple MetaResonance units for charging phone, tablet, medical devices, battery banks, and the power-tool battery.

We designed the receiver power management circuit as shown in Fig. 5 with three core parts: the impedance matching, rectifier, and customized dc–dc converter with different output voltage, such as the 5 V output for iPad and iPhone charging applications. Fig. 6 shows the Class-D power amplifier operating at 6.78 MHz, and the designed receivers with different output voltages used in the experiment, i.e., 24 V in individual MetaResonance units and the power bank battery, 5 V for tablet, phone, and blood press monitor usage.

For the various device charging applications that are demonstrated in the section on "Applications of MetaResonance-based Wireless Charging Surface," each receiver has a fabricated plastic stand designed with Solidworks and fabricated with a 3-D printer. The receiver circuit and receiver coils are installed inside the plastic stand.

B. Power Distribution With One MetaResonance Unit

We first show the possible customization of the power pattern and improvement achieved in the power efficiency of one MetaResonance unit. We consider different configurations, labeled as `config` in Fig. 1(c). The architecture of a MetaResonance unit is shown in Fig. 1(b), and the prototype of this unit is shown in Fig. 8(a) and (b). The setup shown in Fig. 8(a) aids in measuring the magnetic field distribution using oscilloscope measurements with the open voltage of the receiver coil (reference coil). The second setup shown in Fig. 8(b) is for measuring the actual received power on a load resistor. In our prototype, the power distribution layer and the meta-resonance layer are

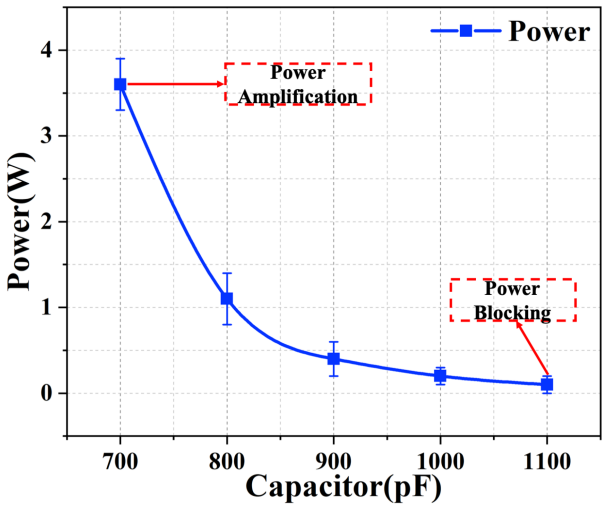

Fig. 7. Power change with different connected capacitance at corner of the surface.

separated by $h = 2$ cm, while the gap between meta-resonance layer and the receiver coil is 3 cm. The power source is provided by Class-D power amplifier with maximum 30 W and 6.78 MHz working frequency [5]. Additionally, the meta-resonance layer consists of 12 meta-cell array of the coils in three rows, and all meta-cells are equally separated by 0.5 cm from each other .

The simulation results for the normalized magnetic field distribution over one MetaResonance unit are presented in subfigures (config1-1) to (config5-1). These are obtained from COMSOL Multiphysics [31], where we define normalized magnetic field distribution as the ratio of magnetic field values of each point to the maximum permissible value in the simulation. The experimental results of the magnetic field distribution with oscilloscope measurement are shown in subfigures (config1-2) to (config5-2), and the power distribution pattern with load measurement are shown in subfigures (config1-3) to (config5-3).

We first study the current power distribution limitation in config1, shown in Figs. 8 (config1-1), (config1-2), and (config1-3). All meta-cell coil units at the meta-resonance layer are placed in open circuit, which is has the same effect of connecting a transmitter coil to a power source, which is similar to the methodology followed in the state-of-the-art works [24], [25]. The magnetic field and received power results shown in Fig. 8 (config1-1),(config1-2), (config1-3) reveal that power is maximized at the center of the coil and decreases as we move radially outward. This concentric pattern not only stays fixed regardless of capacitance changes within the coils in the power distribution layer, but also majorly impacts the received power at the charging electronic devices placed anywhere on the surface. Hence, to create custom varying energy patterns based on the locations of the receivers on a surface, the energy field needs to be dynamically reshaped. The goal at any given time is to maximize the power density at the cells under the locations of the receivers as well as block the power over the other cells for both user-safety and to increase end-to-end power transfer efficiency. Subfigures (config2-1), (config2-2), (config2-3) provide simulation and experimental results for dynamically varying power distributions with the meta-resonance layer. These correspond to optimal energy patterns for delivering power wirelessly, for different numbers and locations of devices over the surface. Notably, these results also reveal that the power at the corner is improved from 0 to 5 W by applying the meta-cells, which show the outstanding performance of increasing the power transfer density and, accordingly, charging distance. Based on the above theory and using (13), we can select capacitor values of the meta-resonance layer such that the meta-cell coil at the left bottom corner amplifies the power, the meta-cell coils in the center allows the power to normally pass with open coil connections, with remaining cells blocking the power. The capacitance value of the meta-cell could be found through the following two scenarios: 1) the received power from the corner of the transmitter can be maximized; and 2) the power passing through the center of the transmitter can be blocked. With the capacitor value range from the Fig. 3 as a reference, the power change from the receiver as shown in Fig. 8(b) and the corresponding capacitor are plotted in Fig. 7.

The results show that a meta-cell connected by a capacitor with around 700 pF maximizes the received power at the corner, which only has a 30 pF difference compared with the theoretical value. This error is acceptable in the experiments. Besides, we can find that the received power is close to 0 with a connected capacitance of 1100 pF. The plotted trend demonstrates that capacitance bigger than 1100 pF has better performance of power blocking.

Given the multiple experimental results, in the following implementation, the average capacitor values of the meta-cell for power amplification and power blocking are determined as 707 and 1120 pF, respectively. In the same way, Fig. 8 (config3-1), (config3-2), and (config3-3) shows we maximize the power under the four corner locations with power blocking for the rest. Additional, the received power at Fig. 8 (config3-3) is lower than received power shown in Fig. 8 (config1-3), and (config2-3). This is because the received power is divided into four parts and four charging devices can get power at these positions simultaneously. For the whole surface, we see that 12 spots are created in the Fig. 8 (config4-1), (config4-2), and (config4-3), with the maximal possible power delivered in each spot. As before, since the input power is divided into 12 parts, the power at each spot is lower than the the power shown in Fig. 8 (config1-3), (config2-3), and (config3-3). Here, 12 devices can be charged at same time. This method maximizes the utilization of the power, increases the power efficiency, and reduces the power loss in regions of the surface without devices. In the last configuration shown in Fig. 8 (config5-1), (config5-2), and (config5-3), we observe that the meta-surface blocks the power over the whole surface. Here, the power delivery decreases by more than 95%, which isolates interference caused by the magnetic field [32], and thus, ensures the human safety not impacted by strong magnetic fields [33], [34]. Furthermore, the voltage and current of receiver load as a function of the length over the surface are obtained under each configuration (config1-5) and are shown in Fig. 8(d). Specifically, in config1 , 5, voltage

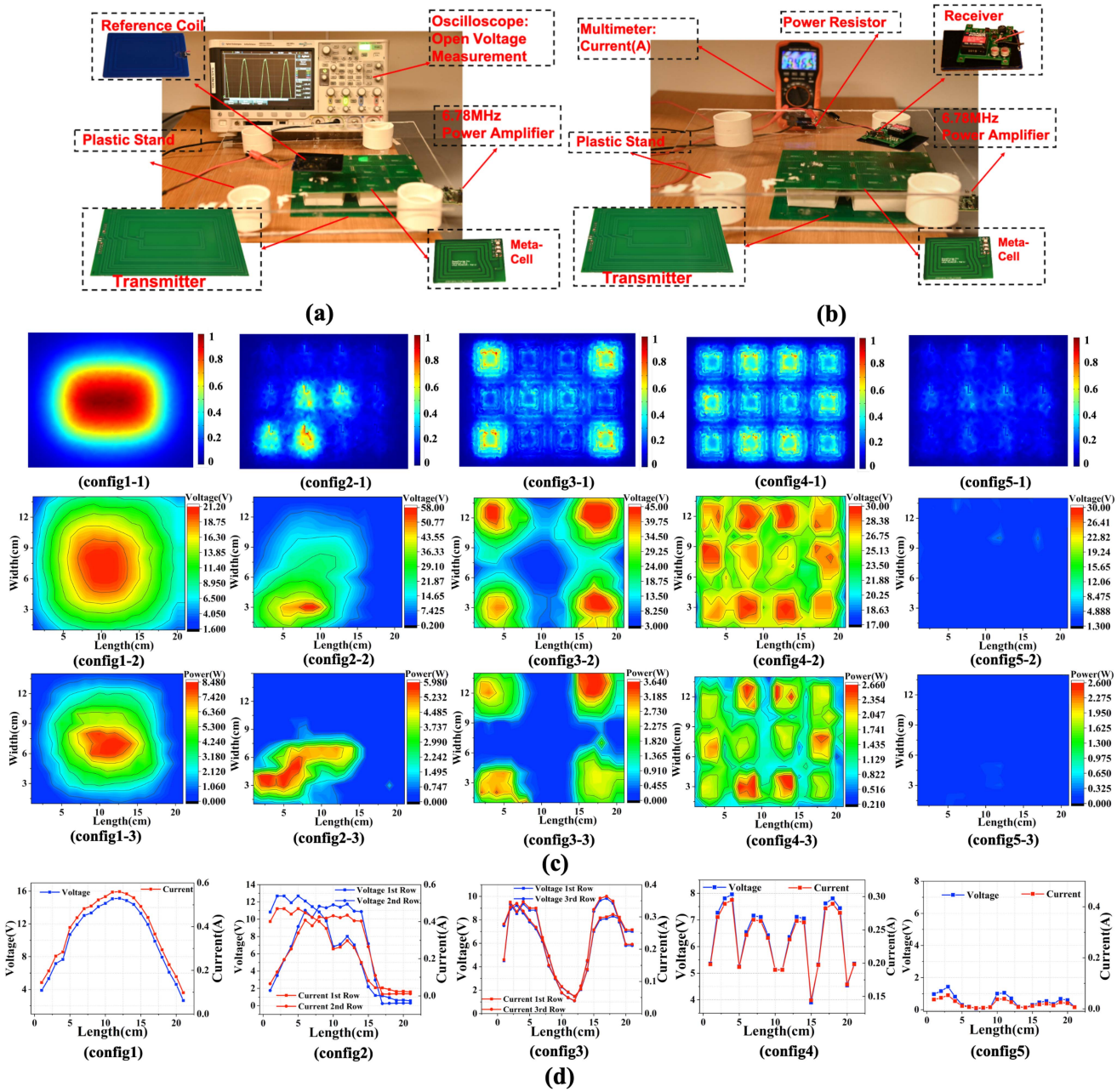

Fig. 8. MetaResonance unit experiment set-up showing (a) magnetic field distribution based on the open voltage of reference coil, (b) power distribution based on the received power of the load resistor, (c) magnetic field and the power distribution of one MetaResonance unit with different configurations, and (d) the voltage and current change under different configuration. In (c), the first, second and third rows provide simulation and experiment results for different wireless power transfer configurations. As shown, `config1` shows the power pattern with the MetaResonance layer layer with an open circuit; `config2-4` shows the power patterns of different spots with a customized MetaResonance layer; `config5` demonstrates the power blocking with human safety via the MetaResonance layer. In (d), the voltage and current is obtained from the load connected to the receiver.

and current values are recorded from one edge to the cross edge through the center of the meta-cell array at the second row; in `config2,3,and4`, the corresponding voltage and current are measured from one edge to the cross edge through the center of the meta-cell array at: first and second row, first and second row, and the second row, respectively. Based on the results of simulation and experiments, we notice that the power distribution is not a uniform pattern, this is because the meta-cell would not change the location-dependence property of the power distribution pattern from meta-cell to receiver, as proved by (14).

With the redistributed power pattern, we experimentally studied the power transfer efficiency, such as the end-to-end power efficiency and dc–dc efficiency, with meta-cell and the loss analysis for power amplification, power blocking and power normally passing. We define the end-to-end power efficiency in one MetaResonance unit as the ratio between the received power at the reference coil and the output power of the

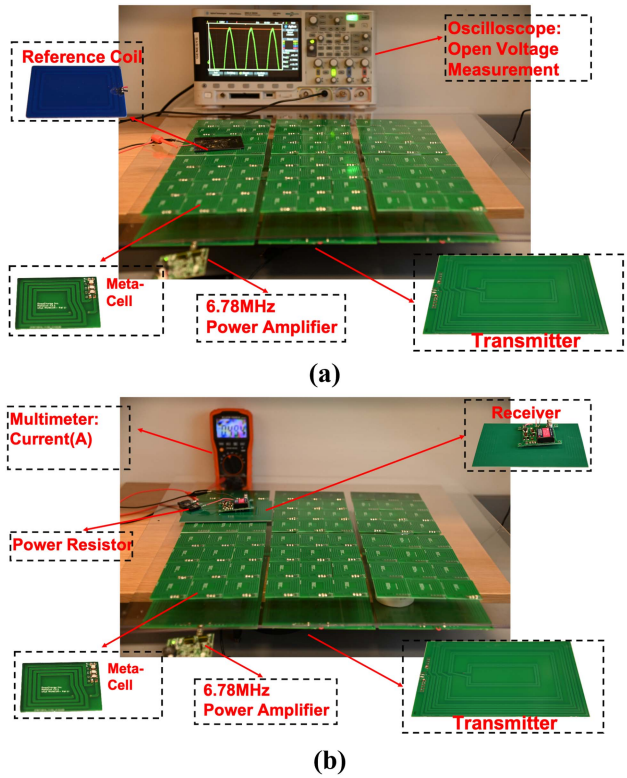

Fig. 9. Multiple MetaResonance units experimental setup. (a) Magnetic field distribution measurement based on the open voltage of reference coil with oscilloscope. (b) Power distribution measurement based on the received power of the load resistor with voltage meter.

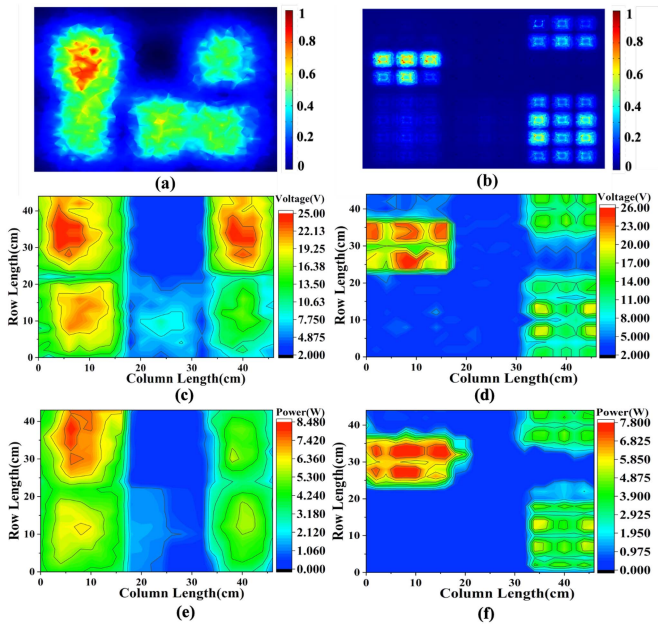

Fig. 10. Magnetic field and power distribution of surface with the combination of energy hopping and meta-surface layer. Results show how the meta-surface layer allows the wireless power transfer over a large surface. (a), (c), and (e) depict the magnetic field and power patterns via simulation (a) and experiments (c), (e). (b), (d), and (f) depict the magnetic field and power patterns via simulation (b) and experiment (d), (f).

amplifier. Accordingly, the end-to-end power efficiency for the first configuration (`config 1`) is obtained as 34%. Similarly, for `config` 2,3, and 4 this is 92.8%, 72%, and 48%, respectively. DC–DC efficiency for one MetaResonance unit is defined as the ratio between the received power on the load of the receiver [shown in Fig. 8(b)] and the input power of the power amplifier. Similar to the end-to-end power efficiency, four configurations are considered, the obtained dc–dc efficiency are 31%, 81.2%, 62%, and 41% for `config` 1, 2, 3, and 4, respectively. We note that the dc–dc efficiency is lower than the end-to-end power efficiency due to the loss from the dc–dc converter in the receiver power management circuit. With end-to-end and dc–dc energy efficiency, we note that the power efficiency decreases as the number of receivers increases. In particular, for the case with more number of devices, the source power distributed over more locations. As opposed to this, for the case with lower number of devices, power is concentrated over fewer locations. In addition, compared to the case with no meta-resonance (`config 1`), we see significant improvement in end-to-end power efficiency. As an example, for the case of no-meta-resonance, we have power distributed regardless of the receiver location in a concentric manner based on the physical characteristics of the coil.

In the experiment, the intrinsic resistance of the meta-cell leads to the loss (P_{loss}). In the scenario of power normally passing, the power loss is 0 since the meta-cell is an open circuit and no current is circulating inside the meta-cell. The loss can be calculated via the the current circulating (I) inside the meta-cell and the intrinsic resistance $P_{loss} = I^2 R_{intr} = (|V/Z|)^2 R_{intr}$. Here, V is the measured voltage inside the meta-cell, $Z = R_{intr} + j\omega L - \frac{1}{j\omega C}$ is the impedance of the meta-cell, L is the inductance,C is the capacitance of the connected capacitor, and ω is the working frequency. The fabricated meta-cell has intrinsic resistance $R_{intr} = 0.1\,ohm$, inductance $L = 0.388\mu$H, and $C = 1120$ pF. The maximum power loss of individual meta-cell for power amplification and power blocking could be calculated as $P^a_{loss} = 0.058$ W and $P^b_{loss} = 0.01$ W, respectively. The total loss distribution with N meta-cell would be calculated as NP_{loss}. The quality of the fabrication highly impacts these losses. Therefore these losses can be optimized by adjusting the thickness or the number of the turns of meta-cell. In the practical use case, these losses are acceptable for power amplification and blocking.

C. Power Distribution With Multiple MetaResonance Units

Based on the performance of an individual MetaResonance unit, this section extends the study for a large surface with multiple MetaResonance units. The power propagates along the (bottom) power distribution layer via energy hopping among transmitter coils, while the meta-resonance layer controls the power redistribution over the (top) meta-resonance layer. The architecture of the multiple MetaResonance units on a large surface is depicted in Fig. 1(a), where only the first transmitter resonator is connected to the power source. The power from source resonator propagates to different resonators within the same layer. Our experimental setup for a large surface is shown in Fig. 10, which is composed of six MetaResonance units in

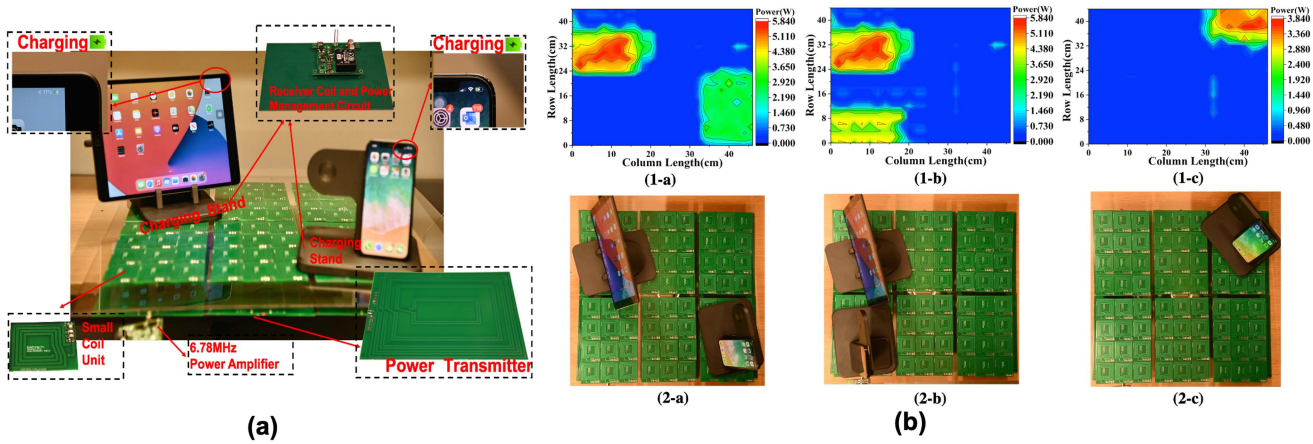

Fig. 11. (a) Experimental setup for MetaResonance wireless power transfer over the surface. (b) Tablet and phone charging at different locations.

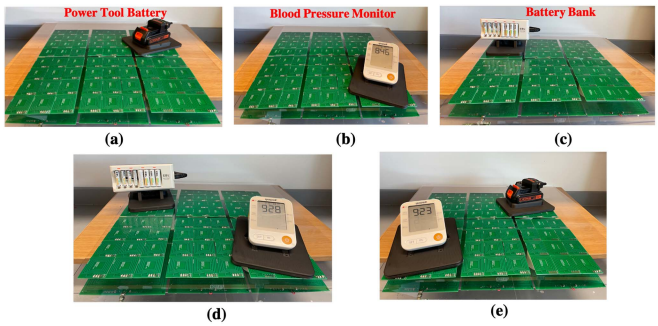

Fig. 12. MetaResonance wireless power transfer surface application with different types of devices, including power-tools battery, blood pressure monitor, and different battery banks.

two rows and three columns. The tuple labels are as given in Fig. 1, where the resonator that is connected to the power amplifier is identified as (1,1). The power amplifier is same as the one in the previous section with maximum 30 W input power and 6.78 MHz working frequency. The distance between the power distribution and the meta-resonance layers is $h = 5$ cm, the edge-to-edge gap between transmitter coils is 1.5 cm, and the separation between meta-cell coils in the meta-resonance layer is 0.5 cm. We have fabricated and used over 72 meta-cell coils in this test. Here, the flow within the power distribution layer has two active paths: (1,1)-(1,2)-(1,3)-(2,3), and (1,1)-(2,1). The approach of how to create these two paths are based on the impedance analysis of the energy hopping of our previous work, which are not explained here. The connected capacitors for each transmitter are given as [110, 135, 115, 120, 0, 130 pF] for transmitter with tuples[(1,1),(1,2),(1,3),(2,1),(2,2),(2,3)], respectively.

To study the power transfer performance using the MetaResonance surface, we first conduct perform extensive simulations, followed by experimental validations. The first experimental setup is shown Fig. 9(a), where the meta-cell coils on the top layer are set to open voltages. This situation is identical to traditional energy hopping. We measure the open voltage at the reference coils (same coils as on MetaResonance unit) via an oscilloscope, The second experimental setup maps the power distribution over the meta-resonance layer based on the load resistor. Here, the receiver coil in this experiment has size 10 cm $*$ 15.5 cm and inductance 1.2 μH. We used a larger receiver coil to ensure higher received power, longer transfer distance, and larger overlap area between the receiver and transmitter coils. Using this configuration without the meta-resonance layer, Fig. 10(a) shows the normalized COMSOL simulation results for open voltage meta-resonance layer. We note that only the transmitters (1,1), (1,2), (1,3), (2,1) and (2,3) provide power. Furthermore, Fig. 10(c) and (e) shows the experimental results for the reference coil voltage and the received power at the load resistor for the same configuration as Fig. 10(a).

We note that the energy field is either present over the entire area of a transmitter coil or it is totally absent. No customization of energy patterns, amplification of power, and blocking capability is possible over the surface. On the other hand, Fig. 10(b) shows the COMSOL simulation results for normalized magnetic field over surface with an active meta-resonance layer. Fig. 10(d) and (f) shows the experimental results for the reference coil voltage and the received power at the load resistor for the same configuration as b. Furthermore, we can customize the energy patterns with high granularity and create variable sized areas of blocked power. For example, the measured voltage on the transmitter coil (1,1) decreases from 22 V for the nonmeta-resonance case [see Fig. 10(c)] to almost zero with the meta-resonance blocking [see Fig. 10(d)]. Also, the received power from transmitter coil (1,1) decreases from 7 W to 0 W, as shown in Fig. 10(e) and Fig. 10(f) by utilizing meta-resonance blocking.

D. Applications of MetaResonance-Based Wireless Charging Surface

The validation results so far indicate the benefits of MetaResonance-based wireless charging system, including customized energy patterns, amplification and blocking of power with enhanced human safety and end-to-end efficiency. Next, we explore the usage of the MetaResonance power transfer system for charging consumer electronics, such as a phone (iPhone) and tablet (iPad). Second, we show the charging performance of medical devices, such as blood pressure monitor, industrial tools

that include power-tool battery packs, and a battery bank. We use the same experimental setup from the multiple MetaResonance unit experiments, as shown in Fig. 11 for iPad and iPhone charging. We update the receiver output voltage to 5 V and use a high efficient dc–dc converter to have a stable output. We design 3-D printed enclosure stands to enclose all electronic components, as shown in Fig. 11. The iPad and iPhone with their stands are placed at different locations and the corresponding experimentally observed energy patterns over the surface are presented in Fig. 11(b). In the first configuration, the iPad receives up to 5.2 W power and phone receives about 2.9 W power in real time. In the second configuration, iPad gets around 5.5 W received power, and phone gets 3.6 W. Finally, in the third configuration, the iPhone gets 3.6 W power.

The proposed MetaResonance wireless charging system is not limited to only these example consumer electronics devices; rather it can be used for wide range of various application as shown in Fig. 12. These include industrial tools (batteries for power-tools), medical devices (blood pressure monitor), and different sized battery bank, to name a few. Each device can be placed at random positions on the charging surface [see examples shown in Fig. 12(a)–(c)]. As before, only the area under the devices deliver power and charge the devices. The rest of the areas are blocked via the meta-surface layer. Fig. 12(e) and (d) demonstrates the possibility of simultaneous multidevice surface charging of the blood pressure monitor and battery packs.

V. Conclusion

This article introduced *MetaResonance*, the first-of-its-kind fully reconfigurable surface for wireless power transfer system. We explained the theory, conducted extensive simulations and experimental results, as well as demonstrated practical use-cases involving consumer electronics and medical device charging. The MetaResonance surface was capable of creating customizable power patterns with fine granularity by reshaping the power distribution over the layer of transmitter coils. Results demonstrated that highly tuned wireless power patterns were possible with different and controllable configurations of the meta-resonance layer. In addition, results showed that the meta-resonance layer addressed the concerns of human safety, while increasing the end-to-end power transfer efficiency up to 92.8%.

References

[1] A. Kurs, A. Karalis, R. Moffatt, J. D. Joannopoulos, P. Fisher, and M. Soljačić, "Wireless power transfer via strongly coupled magnetic resonances," *Science*, vol. 317, no. 5834, pp. 83–86, 2007.

[2] C. K. Lee, W. X. Zhong, and S. Y. R. Hui, "Effects of magnetic coupling of nonadjacent resonators on wireless power domino-resonator systems," *IEEE Trans. Power Electron.*, vol. 27, no. 4, pp. 1905–1916, Apr. 2012.

[3] J. Qu, L. He, N. Tang, and C.-K. Lee, "Wireless power transfer using domino-resonator for 110-kv power grid online monitoring equipment," *IEEE Trans. Power Electron.*, vol. 35, no. 11, pp. 11380–11390, Nov. 2020.

[4] K. Li, U. Muncuk, M. Y. Naderi, and K. R. Chowdhury, "Softcharge: Software defined multi-device wireless charging over large surfaces," *IEEE Trans. Emerg. Sel. Topics Circuits Syst.*, vol. 10, no. 1, pp. 38–51, Mar. 2020.

[5] K. Li, Y. Naderi, U. Muncuk, and K. R. Chowdhury, "isurface: Self-powered reconfigurable intelligent surfaces with wireless power transfer," *IEEE Commun. Mag.*, vol. 59, no. 11, pp. 109–115, Nov. 2021.

[6] K. Li, U. Muncuk, M. Y. Naderi, and K. R. Chowdhury, "Isense: Intelligent object sensing and robot tracking through networked coupled magnetic resonant coils," *IEEE Internet Things J.*, vol. 8, no. 8, pp. 6637–6648, Apr. 2021.

[7] J. Jadidian and D. Katabi, "Magnetic mimo: How to charge your phone in your pocket," in *Proc. 20th Annu. Int. Conf. Mobile Comput. Netw.*, 2014, pp. 495–506 .

[8] L. Shi, Z. Kabelac, D. Katabi, and D. Perreault, "Wireless power hotspot that charges all of your devices," in *Proc. 21st Annu. Int. Conf. Mobile Comput. Netw.*, 2015, pp. 2–13 .

[9] M. Song et al., "Wireless power transfer based on novel physical concepts," *Nature Electron.*, vol. 4, no. 10, pp. 707–716, 2021.

[10] Z. Li, X. Tian, C. W. Qiu, and J. S. Ho, "Metasurfaces for bioelectronics and healthcare," *Nature Electron.*, vol. 4, no. 6, pp. 382–391, 2021.

[11] J. Zhou, P. Zhang, J. Han, L. Li, and Y. Huang, "Metamaterials and metasurfaces for wireless power transfer and energy harvesting," *Proc. IEEE*, vol. 110, no. 1, pp. 31–55, Jan. 2022.

[12] G. Zheng, H. Mühlenbernd, M. Kenney, G. Li, T. Zentgraf, and S. Zhang, "Metasurface holograms reaching 80% efficiency," *Nature Nanotechnol.*, vol. 10, no. 4, pp. 308–312, 2015.

[13] S. Lepeshov and A. Krasnok, "Tunable phase-change metasurfaces," *Nature Nanotechnol.*, vol. 16, no. 6, pp. 615–616, 2021.

[14] K. Li et al., "Nanoscale light confinement and nonlinearity of hybrid plasmonic waveguide with a metal cap," *Opt. Eng.*, vol. 54, no. 10, 2015, Art. no. 107101.

[15] A. S. Solntsev, G. S. Agarwal, and Y. S. Kivshar, "Metasurfaces for quantum photonics," *Nature Photon.*, vol. 15, no. 5, pp. 327–336, 2021.

[16] K. Li et al., "Discrete talbot effect in dielectric graphene plasmonic waveguide arrays," *Carbon*, vol. 118, pp. 192–199, 2017.

[17] W. Du et al., "Electrically controllable directional coupler based on tunable hybrid graphene nanoplasmonic waveguide," *Opt. Commun.*, vol. 430, pp. 450–455, 2019.

[18] P. Sun et al., "Sensitivity enhancement of surface plasmon resonance biosensor based on graphene and barium titanate lauers," *Appl. Surf. Sci.*, vol. 475, pp. 342–347, 2019.

[19] B. Salehihikouei et al., "Deep learning on multimodal sensor data at the wireless edge for vehicular network," *IEEE Trans. Veh. Technol.*, to be published, doi: 10.1109/TVT.2022.3170733.

[20] H. Zhao, Y. Shuang, M. Wei, T. J. Cui, P. Del Hougne, and L. Li, "Metasurface-assisted massive backscatter wireless communication with commodity wi-fi signals," *Nature Commun.*, vol. 11, no. 1, pp. 1–10, 2020.

[21] B. Wang, W. Yerazunis, and K. H. Teo, "Wireless power transfer: Metamaterials and array of coupled resonators," *Proc. IEEE*, vol. 101, no. 6, pp. 1359–1368, Jun. 2013.

[22] Z. Zhang, H. Pang, A. Georgiadis, and C. Cecati, "Wireless power transfer–an overview," *IEEE Trans. Ind. Electron.*, vol. 66, no. 2, pp. 1044–1058, Feb. 2019.

[23] G. G. Buchmeier, A. Takacs, D. Dragomirescu, J. Alarcon Ramos, and A. Fortes Montilla, "Optimized NFC circuit and coil design for wireless power transfer with 2D free-positioning and low load sensibility," *Sensors*, vol. 21, no. 23, 2021, Art. no. 8074.

[24] S. Li and C. C. Mi, "Wireless power transfer for electric vehicle applications," *IEEE J. Emerg. Sel. Top. Power Electron.*, vol. 3, no. 1, pp. 4–17, Mar. 2015.

[25] X. Mou and H. Sun, "Wireless power transfer: Survey and roadmap," in *Proc. IEEE 81st Veh. Technol. Conf. (VTC Spring)*, 2015., pp. 1–5.

[26] X. Yu, S. Sandhu, S. Beiker, R. Sassoon, and S. Fan, "Wireless energy transfer with the presence of metallic planes," *Appl. Phys. Lett.*, vol. 99, no. 21, 2011, Art. no. 214102.

[27] X. Yu, T. Skauli, B. Skauli, S. Sandhu, P. B. Catrysse, and S. Fan, "Wireless power transfer in the presence of metallic plates: Experimental results," *AIP Adv.*, vol. 3, no. 6, 2013, Art. no. 062102.

[28] H. Haus, *Waves and Fields in Optoelectronics*. Hoboken, NJ, USA: Prentice-Hall, 1984, p. 402.

[29] S. Assawaworrarit, X. Yu, and S. Fan, "Robust wireless power transfer using a nonlinear parity-time-symmetric circuit," *Nature*, vol. 546, no. 7658, pp. 387–390, 2017.

[30] J. J. Casanova, Z. N. Low, J. Lin, and R. Tseng, "Transmitting coil achieving uniform magnetic field distribution for planar wireless power transfer system," in *Proc. IEEE Radio Wireless Symp.*, 2009, pp. 530–533.

[31] COMSOL Multiphysics, 2022. [Online]. Available: https://www.comsol.com

[32] S. Kong et al., "An investigation of electromagnetic radiated emission and interference from multi-coil wireless power transfer systems using resonant magnetic field coupling," *IEEE Trans. Microw. Theory Techn.*, vol. 63, no. 3, pp. 833–846, Mar. 2015.
[33] J. C. Lin, "Wireless power transfer for mobile applications, and health effects [telecommunications health and safety]," *IEEE Antennas Propag. Mag.*, vol. 55, no. 2, pp. 250–253, Apr. 2013.
[34] T. Sasatani, A. P. Sample, and Y. Kawahara, "Room-scale magnetoquasistatic wireless power transfer using a cavity-based multimode resonator," *Nature Electron.*, vol. 4, no. 9, pp. 689–697, 2021.

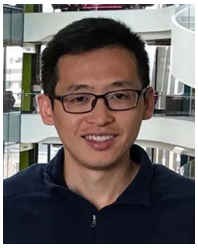

Kai Li received the B.S. and M.S. degrees in physics from Qingdao University, Qingdao, China, in 2014 and 2017, respectively, and the Ph.D. degree in electrical and computer engineering from Northeastern University, Boston, MA, USA, in 2021.

He is a Postdoc with Electrical and Computer Engineering Department, Northeastern University. His research interests include plasmonics, wireless power transfer, quantum communication, wireless mesh networks communication.

Dr. Li was the recipient of the Best Paper Awards at IEEE GLOBECOM in 2019.

M. Yousof Naderi received the Ph.D. degree in electrical and computer engineering from Northeastern University, Boston, MA, USA, in 2015.

He is currently a Research Assistant Professor with the Electrical and Computer Engineering Department, Northeastern University. His research interests include the design and development of software-defined wireless systems, wireless energy transfer and harvesting, and wireless communications.

Dr. Naderi was the recipient of NEU Ph.D. dissertation award in 2015, Best Paper Awards at the IEEE INFOCOM in 2018, and IEEE GLOBECOM in 2019.

Ufuk Muncuk received the Ph.D. degree in electrical and computer engineering from Northeastern University, Boston, MA, USA, in 2019.

He is currently a Research Assistant Professor with the Electrical and Computer Engineering Department, Northeastern University. His research interests include RF energy harvesting and wireless power transfer.

Dr. Muncuk was the recipient of the Best Paper Runners-up at ACM SenSyS 2018, Best Paper Awards at IEEE ICC in 2013, and IEEE GLOBECOM in 2019.

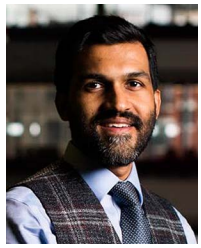

Kaushik Roy Chowdhury (Senior Member, IEEE) received the M.S. degree from the University of Cincinnati, Cincinnati, OH, USA, in 2006, and the Ph.D. degree from the Georgia Institute of Technology, Atlanta, GA, USA, in 2009.

He is currently a Professor with the Electrical and Computer Engineering Department, Northeastern University, Boston, MA, USA. His current research interests include deep learning in wireless networks, wireless RF energy harvesting and IoT, and intra/on-body communication.

Dr. Chowdhury was the recipient of the Presidential Early Career Award for Scientists and Engineers (PECASE) in 2017, ONR Director of Research Early Career Award in 2016, and the NSF CAREER Award in 2015.